IEEE Access
Multidisciplinary ⋮ Rapid Review ⋮ Open Access Journal

Received 12 October 2022, accepted 26 October 2022, date of publication 1 November 2022, date of current version 8 November 2022.

Digital Object Identifier 10.1109/ACCESS.2022.3218669

RESEARCH ARTICLE

The Mitigation of Eddy-Current Losses in Ferromagnetic Samples Produced by Laser Powder Bed Fusion

AINO MANNINEN, JENNI PIPPURI-MÄKELÄINEN, TUOMAS RIIPINEN, TOMI LINDROOS, SINI METSÄ-KORTELAINEN, AND ATTE ANTIKAINEN

VTT Technical Research Centre of Finland Ltd., 02044 Espoo, Finland

Corresponding author: Aino Manninen (aino.manninen@vtt.fi)

This work was supported in part by the Academy of Finland under Grant 330063.

ABSTRACT We study the use of topology optimization in the design of low-loss ferromagnetic core structures for additively manufactured electrical machines. The test case was a simple toroid core with a primary and a secondary winding. A 2D axisymmetric finite element method model was implemented for the toroid, and the core topology was optimized for minimum losses and maximum secondary flux linkage. The optimized core was then modified for additive manufacturing, and test samples were built via laser powder bed fusion. The B-H characteristics and losses of the core were measured in several operation points. The losses were compared against an additively manufactured solid core, a laminated core, and an additively manufactured core with evenly placed air gaps (i.e., grooves). The results show that the losses in the topology-optimized core are on the same level as the losses in the laminated core and considerably smaller than those in the solid core, which is a considerable improvement to previous published works.

INDEX TERMS Eddy currents, magnetic cores, optimization, soft magnetic materials, three-dimensional printing.

I. INTRODUCTION

The active parts of rotating electrical machines comprise windings, cores, and possibly permanent magnets. The cores are typically composed by stacking thin, insulated electrical steel sheets together to fortify the magnetic flux and to mitigate the eddy-current losses. While this approach has its proven benefits, it is best fitted to creating essentially 2D magnetic circuit designs, such as those of radial flux electrical machines. The preparation of the laminated ferromagnetic cores includes several steps—for example, casting, rolling, cutting, welding, and heat treatment—which make the whole process rather rigid and laborious. The desired shape of the electrical steel sheets is attained by punching or laser cutting. During the cutting process, a considerable amount of material is wasted. Further, these processes deteriorate the electromagnetic characteristics of the steel sheets, especially near the cut edges [1].

In comparison with traditional manufacturing methods, additive manufacturing (AM) or 3D printing provides unparalleled design freedom. Recently, the AM of electrical machines has gained a lot of interest in the research community [2], [3]. AM can be used to manufacture ferromagnetic cores [2], coils [4], permanent magnets [5], and also supporting structures for electrical machines [6].

However, one major challenge exists that in practice prevents the wider usage of the currently available AM technologies in manufacturing the ferromagnetic cores of electrical machines. The present AM cores typically suffer from high eddy current losses due to their massive structures without any insulating layers between the ferromagnetic material. As a result, these cores are not competitive to the traditional laminated cores.

In order to improve the performance of AM produced cores, the eddy current issue should be considered during both

The associate editor coordinating the review of this manuscript and approving it for publication was Huaqing Li.

the design of the cores and when choosing the material and AM method. Present AM techniques for ferromagnetic cores include laser powder bed fusion (PBF-LB, also abbreviated as L-PBF), binder jetting (BJT), material extrusion (MEX), also known as fused deposition modeling (FDM), and laminated object manufacturing (LOM) [2]. The most commonly used technology is PBF-LB due to its maturity and because it has been shown to provide a good balance between the mechanical and quasi-static magnetic characteristics of ferromagnetic cores [7]. In order to get good electromagnetic properties, thermal post-processing is required after the printing process [7]. However, though initial demonstrations exist [8], the current PBF-LB technology has limitations in producing thin electrically insulated structures, and therefore, the PBF-LB manufactured cores are typically solid, leading to excessive eddy-current losses, especially at high frequencies [9].

Regarding the alternative options, BJT can produce ferromagnetic cores with high magnetic permeability and increased resistivity [10], but sintering is required after the printing process to densify the structure and to mitigate cracking [10], and the resulting shrinkage has to be taken into account in the design before printing a part. Compared to [7], in [10] the electrical resistivity of the cores was doubled. This increase of the resistivity reduces the losses but not to a level comparable with the laminated cores. MEX is also capable of producing ferromagnetic parts with high resistivity [2], but the saturation magnetization is low [2], [11], and sintering is required after the printing to densify the structure [11]. LOM is a method that could allow printing laminated structures similar to electrical steel sheets, and thus sounds promising in the reduction of the eddy currents. However, currently the material options are limited to copper and stainless steel, the material utilization is equivalent to the processing of laminated steel, and the smallest achievable thickness of the laminated structure might not be small enough to efficiently reduce the eddy current losses. Therefore, this method is not quite ready for the ferromagnetic cores yet [12].

For these reasons, we chose to focus on the PBF-LB technology, and to implement a workflow that can take into account the eddy current mitigation when designing the shape of the ferromagnetic core. With the PBF-LB, the most commonly used soft magnetic materials are Fe-Si or Fe-Co alloys [2]. Fe-Co alloys enable higher saturation magnetic flux density than Fe-Si alloys, but the high price of cobalt can be a restriction, especially in the industrial-scale manufacturing of electrical machines. As our goal was to obtain high power density, we decided to use Fe-Co. A Fe-Co-V material with high-saturation magnetic flux density and reasonably high resistivity [7] was used in this work as a starting point.

To achieve performance that is competitive with traditional laminated cores, the PBF-LB cores should be carefully designed so that the losses are minimized. In literature, introduction of different kind of slits or gaps is proposed [13], [14], [15]. In [13], using computational analysis, the gaps were estimated to reduce the eddy-current losses by 85%, but at the same time, the active core cross-sectional area was reduced, causing the magnetic flux density to drop from 1.5 T to 1.2 T. This suggests that in the core design, there has to be a trade-off between the reduction of losses and the reduction of magnetic flux density. A somewhat similar idea was introduced in [14], where slits were introduced both at the sides of a ring-shaped test core and also inside it. The losses were estimated to lower 17% of those of the bulk material using computational methods. However, the losses in the experimental test core were larger than estimated due to an imperfect structure. Goll et al. [14] also presented the idea of alternating layers of different materials, creating a structure similar to that of a laminated core. A sample core with alternating layers of pure iron and FeAl16 was found to reduce the losses from 4.7 W/kg of pure iron to 0.5 W/kg at 0.2 T and 50 Hz [14]. Annealing treatment was reported to be possible for alternating layered components up to 900 °C for 1 h without losing the effect of the higher resistance separation layers [8]. Higher temperatures resulted in the deterioration of the separation layers and thus higher eddy-current losses. The annealing is important for reducing the hysteresis losses in the soft magnetic materials. In [15], grooves were cut to the rotor air gap surface in order to reduce eddy currents. Peripheral grooving was found to reduce the losses significantly. In [16], a slit structure was proposed to reduce eddy-current losses in a 3D-printed axial flux permanent magnet machine made of soft magnetic composite (SMC). The slits were introduced in the stator core in a similar manner as a laminated structure is used in radial flux machines. However, to this date, the methods for producing the loss mitigating structures have been more of empirical nature and not relying so much on, e.g., numerical optimization.

All the work presented above have attempted to reduce the eddy current losses, nevertheless a clear framework for eddy current mitigation is still missing. In this work, we propose a workflow to consider the eddy current issue by employing topology optimization (TO) [17], [18]. Various TO methods exist in literature, including density based, level set and topological derivatives [19]. For electromagnetic TO, most commonly used method is solid isotropic material with penalization (SIMP) [20], which has been proposed in e.g. [21], [22], [23]. The main advantages of the SIMP method are the continuity of the control variables, which allows to use gradient-based optimization algorithms. A drawback is that SIMP can sometimes leave grey areas (intermediate state between solid and air) which can be hard to realize in practice. Level set method has been used in [24] and [25], and topological derivatives in e.g. [26]. Electromagnetic TO in literature is typically used to e.g. rotor design of electrical machines [21], [22], [23], [26], [27]. Eddy currents have been previously presented as a part of TO in [28], where an induction heater apparatus was optimized in time domain, and the heating power of the eddy currents was maximized.

In this work, we employ the TO method to produce loss mitigating ferromagnetic core design for the fabrication with PBF-LB. As a test case, we use a simple toroid with a primary and a secondary winding. For TO method, we have chosen

material density TO with SIMP due to its simple implementation, and good availability. The purpose is not to further develop any TO method, but to investigate if TO could be used to create loss mitigating core structures. The formulation of the optimization problem and its constraints requires specific attention as the sole minimization of the eddy current losses would lead to an empty space solution. After obtaining loss minimizing structures from TO, we produce samples using PBF-LB. The manufacturability of the TO produced designs is also addressed at this point. Three different samples are manufactured: solid, one with evenly placed grooves, and one designed using TO. The B-H curves and losses of the sample AM cores are measured and compared against the measured losses of a laminated Fe-Co-V core. Finally, the portion of the eddy current losses of the total losses is analyzed via computations to see how much the eddy current losses themselves were reduced. The main novelty of our work is that we introduce a workflow from the design to the additive manufacturing of the eddy current minimizing soft magnetic cores.

II. COMPUTATIONAL METHODS

In this section, we present the electromagnetic model of the toroid core and explain how TO is used to mitigate the core losses. Two different finite element method (FEM) models are employed: the core losses of the produced samples are analyzed with a time-dependent model incorporating the nonlinear magnetic properties whereas the TO is performed with a simplified model assuming sinusoidal time variation (the time-harmonic approach) with linear B-H characteristics.

A. ELECTROMAGNETIC MODEL

The governing equations of the electromagnetic problem are

$$\nabla \times \frac{1}{\mu} (\nabla \times \boldsymbol{A}) = -\sigma \frac{\partial \boldsymbol{A}}{\partial t} + \boldsymbol{J}_\mathrm{e}, \tag{1}$$

where $\boldsymbol{A}$ denotes the magnetic vector potential, μ is the permeability of the material (i.e. $\mu = \mu_\mathrm{r}\mu_0$ where μ_0 is the permeability of vacuum), μ_r is the relative permeability of the material, σ denotes the electrical conductivity of the material, and $\boldsymbol{J}_\mathrm{e}$ denotes the external current density. The magnetic flux density fulfils

$$\boldsymbol{B} = \nabla \times \boldsymbol{A}. \tag{2}$$

In the case of 3D computation, a unique solution is ensured via gauge fixing of the $\boldsymbol{A}$ field:

$$\nabla \cdot (\sigma \boldsymbol{A}) = 0. \tag{3}$$

The permeability, μ, defines the constitutive relation between the magnetic flux density, $\boldsymbol{B}$, and the magnetic field strength, $\boldsymbol{H}$, as $\boldsymbol{B} = \mu \boldsymbol{H}$. During the timedependent analysis of both solid and optimized cores, a B-H curve is used instead of relative permeability for the constitutive relation between $\boldsymbol{B}$ and $\boldsymbol{H}$ in order to take into account the saturation of the ferromagnetic core as

$$\boldsymbol{B} = f\left(\|\boldsymbol{H}\|\right) \frac{\boldsymbol{H}}{\|\boldsymbol{H}\|}, \tag{4}$$

where f is an interpolation function of the single-valued B-H curve.

The external boundaries of the model geometry were given the magnetic insulation boundary condition $\mathbf{n} \times \boldsymbol{A} = 0$ or perfect magnetic conductor boundary condition $\mathbf{n} \times \boldsymbol{H} = 0$, as appropriate for the considered symmetry sector.

In the time-harmonic case, the field quantities are approximated to vary sinusoidally with time, and (1) is reduced to

$$\nabla \times \frac{1}{\mu} (\nabla \times \boldsymbol{A}) = -\mathrm{j}\omega\sigma\boldsymbol{A} + \boldsymbol{J}_\mathrm{e}, \tag{5}$$

where j is the imaginary unit and ω the angular frequency.

The current density in the primary coil domain is

$$J_\mathrm{e} = \frac{N_\mathrm{pw} I_\mathrm{pw}}{A_\mathrm{coil}}, \tag{6}$$

where I_pw is the primary current, N_pw is the number of turns in the primary winding, and A_coil is the cross-sectional area of the current region, perpendicular to the current direction.

The flux linkage is computed as a surface integral of the area inside the coil:

$$\Psi = N_\mathrm{coil} \int_{A_\mathrm{coil}} B_\Psi \mathrm{d}A, \tag{7}$$

where N_coil is the number of turns in the coil, A_coil is the crosssectional area of the coil, and B_Ψ is the out-of-plane magnetic flux density.

The magnetic flux density in the cores is obtained as

$$B = \frac{\Psi_\mathrm{sw}}{N_\mathrm{sw} A_\mathrm{core}}, \tag{8}$$

in which Ψ_sw denotes the flux linkage in the secondary winding, N_sw the number of turns in the secondary winding, and A_core the cross-sectional area of the core. This area is defined by the standard IEC 60404-4 [29] as

$$A_\mathrm{core} = \frac{2m}{\rho\pi\,(D+d)}, \tag{9}$$

in which m denotes the mass of the sample, ρ the density of the sample, D the outer diameter, and d the inner diameter.

The eddy-current losses are calculated in the following way:

$$P_\mathrm{loss} = \int_{V_\mathrm{core}} \frac{1}{\sigma} J^2 \mathrm{d}V. \tag{10}$$

where J is the current density in the core, obtained as $J = -\sigma \frac{\partial \boldsymbol{A}}{\partial t}$ in the time-dependent case and $J = -\mathrm{j}\omega\sigma\boldsymbol{A}$ in the time-harmonic case.

B. TOPOLOGY OPTIMIZATION

In the material density TO method, the material density variable ρ is introduced so that $\rho = 0$ corresponds to air and $\rho = 1$ corresponds to solid material. During TO, the density variable is allowed to have values between 0 and 1 to avoid an integer optimization problem. After TO, the TO problem is fully converged if ρ is either 1 or 0 everywhere and the intermediate values have disappeared.

The density variable affects the material properties in the TO space, in this case, the relative permeability and electrical conductivity. The SIMP method [20] is used for material interpolation in TO, so that a penalized density variable θ_p is obtained:

$$\mu_\mathrm{r} = \mu_\mathrm{r}\theta_\mathrm{p} \tag{11}$$

$$\sigma = \sigma\theta_\mathrm{p} \tag{12}$$

$$\theta_\mathrm{p} = \theta_\mathrm{min} + (1 - \theta_\mathrm{min})\,\rho^p \tag{13}$$

where θ_min is the minimum penalization and p is the penalization power.

The optimization problem is the weighted difference of secondary flux linkage and core losses in order to minimize the losses and maximize the secondary flux linkage:

$$\begin{aligned} &\text{maximize}\, f = K_\Psi \Psi_\mathrm{sw}(\boldsymbol{\rho}) - K_\mathrm{loss} P_\mathrm{loss}(\boldsymbol{\rho}) \\ &st.\ 0 \le \boldsymbol{\rho} \le 1. \end{aligned} \tag{14}$$

$\Psi_\mathrm{sw}(\boldsymbol{\rho})$ is obtained from (7) and $P_\mathrm{loss}(\boldsymbol{\rho})$ from (10) based on the magnetic vector potential solved from the time-harmonic equation (5). The TO problem was solved using the globally convergent method of moving asymptotes (GCMMA) [30]. The GCMMA is a globally convergent version of the method of moving asymptotes (MMA) algorithm. It consists of outer and inner iterations, and each outer iteration can have one or more inner iterations. During outer iteration k, the current estimate of the control variable $\boldsymbol{\rho}_k$ is used to evaluate the objective function, constraints, and their gradients. These are used together with asymptote estimates l_k and u_k to construct an approximating subproblem, which is convex and feasible. The subproblem is passed to inner iterations. During inner iteration j, the subproblem is solved for unique optimum $\boldsymbol{\rho}_{kj}$ The values of objective function and constraints are the solved for $\boldsymbol{\rho}_{kj}$, and if the approximating subproblem is conservative compared to the true function values, the inner iterations are terminated, and $\boldsymbol{\rho}_{kj}$ becomes the next outer estimate $\boldsymbol{\rho}_{k+1}$. Otherwise, a next inner iteration is performed with more conservative approximating subproblem [30].

III. THE DEVELOPMENT OF LOSS-MITIGATING CORE DESIGNS

The idea was to introduce air gaps inside the core in such a way that they would cut the eddy-current paths, thus increasing the effective resistance and decreasing the eddy currents. Furthermore, the aim was also to understand how to balance between eddy-current loss reduction and attainable magnetic flux linkage.

A solid toroid core with an outer and inner diameter of 60 mm and 50 mm, respectively, and a height of 5 mm was chosen as a reference and starting point for the loss-mitigating design developments. A 2D cross-section of the solid toroid core is highlighted in grey in Fig. 1 a. For comparative purposes, a laminated Fe-Co-V core with the same main dimensions as the solid one was manufactured and analyzed as well. The geometry of the laminated stack is highlighted in gray in Fig. 1 b.

Prior to numerical optimization, intuitively proportioned loss-mitigating toroid core designs were prepared. In a solid core, the eddy currents follow a similar trajectory to that of the supply current of the primary winding, and now, simple, evenly placed air gaps were introduced to shorten their path. The geometry of the thereby obtained grooved samples is shown in Fig. 1 c. The width of the grooves is 0.4 mm in the radial direction and 8 degrees in the tangential direction. The distance from groove to groove is 0.5 mm in the radial direction and 0.95 mm from outer boundary to groove on both sides in the radial direction. In the tangential direction, the distance between the grooves is 4 degrees.

Next, TO was used to find out the optimal placement of the air gaps in the core, that is, in the TO design space marked in gray in Fig. 2. The FEM model was 2D axisymmetric with 6831 elements and 16206 degrees of freedom. In the TO design space, a mapped mesh was used with an element size of 0.1 mm, as shown in Fig. 2. Using smaller elements would allow the TO to create smaller details; however, these would be impractical to manufacture.

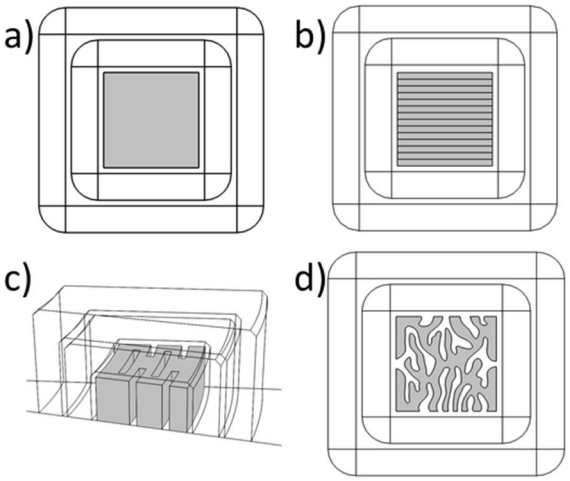

FIGURE 1. Model geometry of (a) a solid sample, (b) a laminated sample, c) a grooved sample, d) a TO DfAM sample, showing the core in grey. The 2D coil geometry is presented in a way that allows defining the in-plane current density in the different parts of the coil separately in the FEM software.

For TO, the core material was assumed to have a relative permeability of 2000, and the supply frequency of the primary winding excitation was set to 500 Hz. A relatively high supply frequency was chosen in order to imitate the presence of higher harmonics in electrical machinery. TO was performed

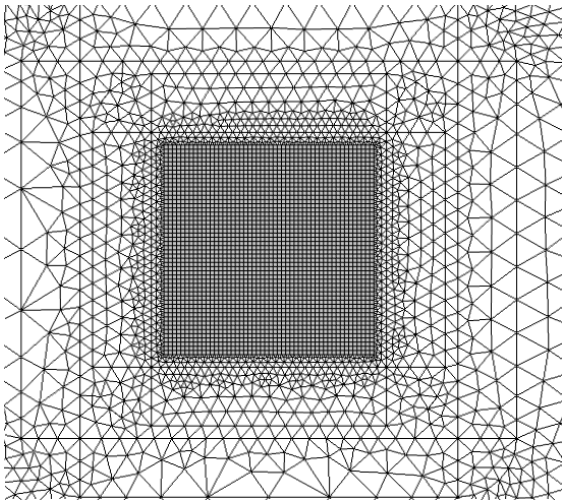

FIGURE 2. Finite element mesh used in the TO.

with $K_\Psi = 1000$ and several values of $K_{\text{loss}} \in [0.01, 2]$ These values were chosen so that K_Ψ was first used to scale the two objectives (flux linkage and losses) to the same magnitude, and after that, K_{loss} was varied in order to get more emphasis on either the flux linkage term or the loss term A balance has to be found between the two terms in the sum, as putting too strong emphasis on the loss minimization will result to empty space solution; in air there are no eddy currents, and therefore also no losses. Minimum penalization θ_{min} was set to 0.001 and penalization power p was set to 1.

The TO problem was solved using COMSOL Multiphysics software [31], and used hardware was two Intel Xeon Gold 5118 CPUs at 2.30 GHz, in total 24 cores and 192 GB of memory. The number of TO variables was 2601. The number of GCMMA outer iterations and function evaluations for the TO to converge is shown in Table 1, with the solution time for different values of K_{loss}.

The result geometries obtained are shown in Fig. 3. Larger K_{loss} values give more weight to the minimization of losses, which shows in the results as decreased volume of the ferromagnetic material. Putting too much weight on loss minimization (i.e., having a too large K_{loss}) will lead to unfeasible geometries with too much material removed as seen in the lower right corner of Fig. 3. On the other hand smaller values of K_{loss} give less weight to loss minimization and more weight to the maximization of the flux linkage. This leads to the larger volume of the ferromagnetic core. The set of TO solutions front obtained by varying K_{loss} is shown in Fig. 4.

From the generated set of solutions, the most promising one was chosen for further study. The highest flux linkage was found with $K_{\text{loss}} = 0.05$, and the losses are on the higher side, but not the highest. Further, the results having small losses also have small flux linkage, which is undesirable. From the manufacturing point of view, $K_{\text{loss}} = 0.05$ is also the most promising. Therefore, this result, outlined in red in Fig. 3, was chosen to be converted into a 3D-printable core geometry.

TABLE 1. TO problem solution information.

K_{loss}	Number of outer iterations	Number of objective function evaluations	Solution time (s)
0.005	192	196	148
0.01	302	308	235
0.05	208	212	161
0.1	656	659	497
0.15	599	602	460
0.2	296	297	233
0.25	279	280	217
0.5	1771	1772	1419
0.75	966	967	761
1	747	748	591
1.5	509	517	405
2	843	861	667

The original TO design, $K_{\text{loss}} = 0.05$ in Fig. 3, had several details that could not have been printed properly that are shown in Fig. 5. Therefore, this design was taken as a starting point, and manually refined into a 3D-printable one. The new design was named TO DfAM (topology-optimized design for AM). Horizontal tabs were changed to have angle of $\geq 45°$. In the lower part of the design, the tabs had to start from the very bottom of the design, as shown in Fig. 5, on the right.

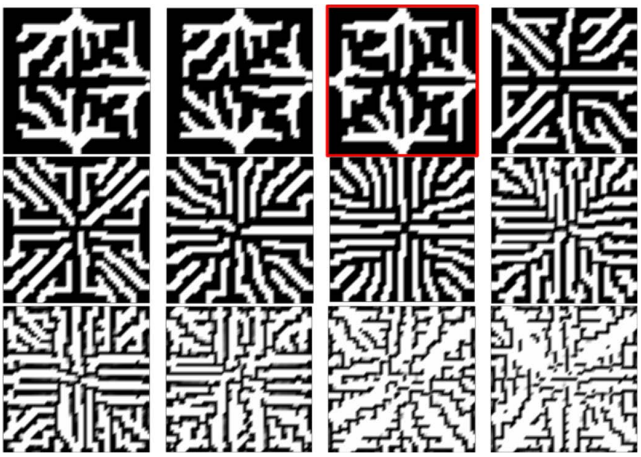

FIGURE 3. Different solutions to the TO problem presented in (14) obtained by varying parameter K_{loss}: top row, from left to right: $K_{\text{loss}} = 0005, 001, 005, 01$; middle row: $K_{\text{loss}} = 015, 02, 02505$; bottom row: $K_{\text{loss}} = 075, 1, 152$ The TO solution initially chosen to be manufactured is marked in red.

While changing the design, the eddy-current losses were evaluated repeatedly and compared with those of the original TO design to ensure that the loss-mitigating effect of the structure was not lost. Also, the gaps in the vertical section on the inner and outer surface of the toroid (see Fig. 5) were manufactured as solid and machined open afterwards. Due to the limitations in the 3D printing technology, the final TO DfAM core shape is quite different from the original TO result. At this point, there was no automated way of converting the TO result to a 3D-printable core shape without manual work. This is something of a drawback in the used

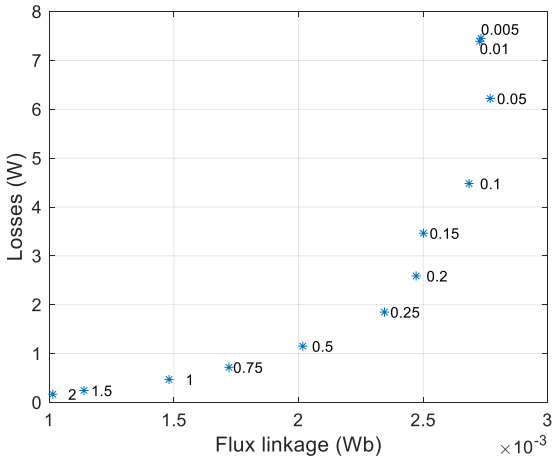

FIGURE 4. Losses against the secondary winding flux linkage for different K_{loss}. K_{loss} values are marked in the figure. Results correspond to the TO solutions presented in Fig 3. Losses and flux linkages were solved by (7) and (10).

method as it adds an extra work stage to the design process. However, here, the TO method served its purpose by helping the designer to come up with new ideas rather than serving the purpose of achieving finalized products. Moreover, even if the TO DfAM differs from the original TO design, it preserves the key features in terms of unique, multiple not fully symmetrically shaped air gaps.

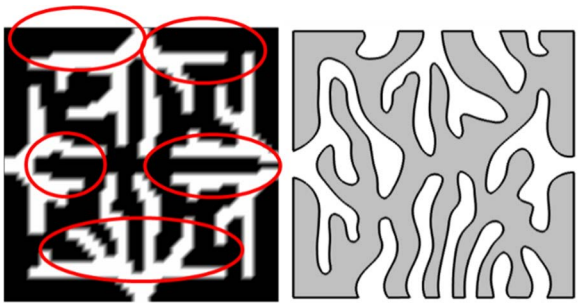

FIGURE 5. Chosen TO result showing examples of unprintable details (on the left). The TO DfAM design is presented for comparison (on the right).

IV. MANUFACTURING, POST TREATMENT, AND THE CHARACTERIZATION OF SAMPLES

Four toroid specimens—one solid, one grooved, and two with a geometry stemming from the TO results—were manufactured with an SLM 125 HL 400W PBF-LB machine from SLM Solutions GmbH. The soft magnetic Fe-49Co-2V powder used was prepared at VTT by gas atomization. The solid and grooved specimens were manufactured at an earlier stage using slightly different powder compositions [32] when compared with the topology-optimized core specimens, which had 0.6 wt% Nb as an alloying element. The feedstock powder was sieved (with a 63 μm opening) and dried in a vacuum furnace overnight prior to manufacturing.

The process parameters used for PBF-LB were: layer thickness = 30 μm, power = 200 W, scanning speed = 775 mm/s, hatch spacing = 80 μm, platform heating = 200 °C, a rotating hatching pattern, and an argon atmosphere for all toroid samples. The specimens were removed from the print platform by electric discharge machining (EDM). The vertical gaps on the inner and outer surface of the TO DfAM sample were machined open, as explained above. Further, the remainder powder was removed from the cavities of the grooved and TO DfAM samples. The built PBF-LB samples are shown in Fig. 6. In the cross-section of the grooved samples, small deviations from the intended geometry were observed (see Fig. 6 c). The lighter green in Fig. 6 c shows the cross-sectional cut of the 3D-printed sample obtained by optical microscopy and the darker-green highlights depict the intended geometry as a CAD model. Fig. 6 d shows the cross-section of the TO DfAM core for a cubic 3D-printed example specimen.

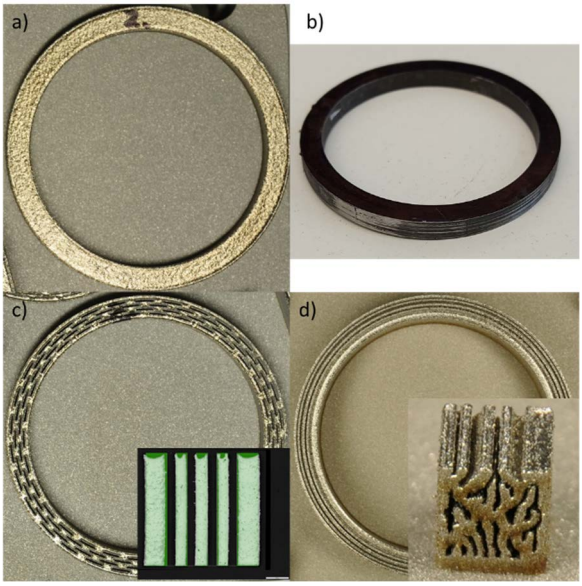

FIGURE 6. Manufactured sample cores: (a) a solid sample, (b) a laminated sample, (c) a grooved sample with its cross-sectional image, the dark green depicting the intended cross-section and the lighter green depicting the manufactured cross-section, (d) a TO DfAM toroid sample and a cube sample showing the cross-section.

Thermal post-processing was applied to the toroid samples. The solid and grooved specimens were annealed at 820 °C for 10 h (HT1). One TO DfAM specimen was heat treated at 700 °C for 2 h, cooled, and then annealed at 820 °C for 10 h (HT2), and the other TO DfAM specimen was annealed at 850 °C for 10 h (HT3). All heat treatments were done in a tube furnace under an Ar+4%H2 atmosphere, and the parts were cooled to 500 °C from the annealing temperature at a rate of 100 °C per 1 h, followed by furnace cooling.

Besides a solid 3D-printed toroid, a laminated toroid reference was manufactured, too. The electrical steel sheet grade was VACOFLUX 50, produced by Vacuumschmelze [33], with a thickness of 0.35 mm. Fourteen sheets were laser cut

to a desired shape and welded together. The built sample was heat treated at 820 °C for 4 h under an Ar+4%H2 atmosphere in accordance with the manufacturer's specifications [33]. The ready-laminated sample is shown in Fig. 6 b.

Primary and secondary windings were wound on the samples in order to perform the magnetic characterization. The numbers of turns in the primary, excitation, winding, and in the secondary, measurement, winding are tabulated in Table 2. The quasistatic DC magnetic characteristics and AC characteristics of the samples were measured according to standards IEC 60404-4 [29] and IEC 60404-6 [34], respectively. During the measurements, the current in the primary winding is controlled in such a manner that a sinusoidal magnetic flux density with a desired amplitude and frequency can be observed from the secondary winding. Altogether, nine different AC operation points were measured at magnetic flux densities 1 T, 1.5 T, and 2 T for frequencies 10 Hz, 50 Hz, and 100 Hz.

The nonlinear magnetic characteristics of the cores were represented by single-valued B-H curves in the time-dependent finite element analysis. These single-valued B-H curves were derived from the quasistatic DC measurement data of the heat-treated samples by taking a limited number of points from the virgin curve, ensuring the monotonicity of the outcome. The thereby obtained B-H curves for all the studied samples are presented in Fig. 7. Possible sources for the small differences between the TO DfAM HT2 sample and the rest of the samples are, for example, slight differences in the sample microstructures [7].

For the electrical resistivity measurements, 90 mm × 10 mm × 10 mm bar samples of Fe-Co-V and Fe-Co-V-Nb powders were manufactured via PBF-LB. The same manufacturing and heat treatment procedures were followed as those that were used with the toroid samples [32], [7]. The electrical resistivity of the Fe-Co-V samples was found to be 43.5 $\mu\Omega$cm while the alloy with niobium addition had a resistivity of 49.4 $\mu\Omega$cm [32], [7]. The former value was applied in the computations of the solid and grooved 3D-printed samples and the latter was applied for the analyses of the TO DfAM samples. The electrical resistivity of the electrical steel sheets was taken from the manufacturer's data sheets: 42 $\mu\Omega$cm [33].

The density of all samples was defined using the value of standard Fe-Co-V alloys (i.e., 8.11 g/cm^3).

V. COMPARISON OF SAMPLES

The AC characteristics (i.e., the losses of the five Fe-Co-V toroid samples) were measured. The eddy-current losses of the four cores—those of the solid, laminated, grooved, and TO DfAM HT2 samples—were also analyzed with a time-dependent FEM. This was done in order to assess the validity of the numerical methods used. Further, with the computed eddy-current losses and the measured total losses, a segregation into loss components (i.e., eddy-current losses and hysteresis plus excess losses) could be performed. To evaluate the performance of the cores, also the secondary flux linkage was

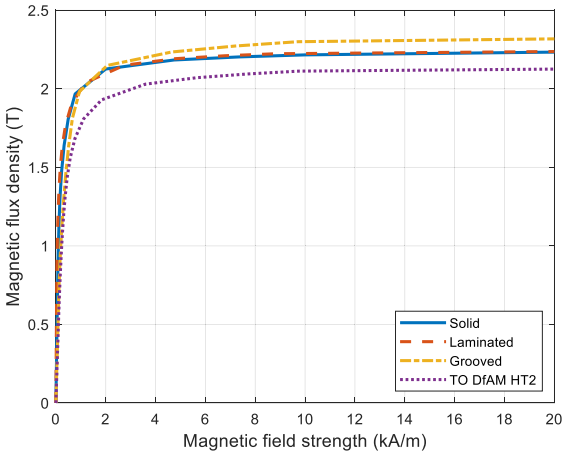

FIGURE 7. Single-valued B-H curves used in the FEM models.

TABLE 2. Key properties of the toroid samples.

Inner diameter (mm)		50
Outer diameter (mm)		60
Height (mm)		5
Solid sample	Number of turns in primary winding	275
	Number of turns in secondary winding	60
Laminated	Number of turns in primary winding	250
sample	Number of turns in secondary winding	25
Grooved sample	Number of turns in primary winding	250
	Number of turns in secondary winding	55
TO DfAM	Number of turns in primary winding	275
samples	Number of turns in secondary winding	60

computed. For the solid, laminated, and TO DfAM samples, a 2D axisymmetric model was used while a 3D analysis had to be performed for the grooved sample, because the grooved geometry is not axisymmetric. The same operation points that were measured were also analyzed through the numerical computations.

The finite element mesh was generated taking into account the skin depth of the cores for each studied case and the meshes for the 2 T, 100 Hz operation point are shown in Fig. 8. The primary current was chosen so that the magnetic field strength matched its measured value. The number of time steps per period was 50 for the laminated and grooved samples and 100 for the solid and TO DfAM samples. Altogether, two periods of supply current were computed.

Fig. 9 and Fig. 10 show the measured and computed B-H curves of the four different samples at the 1.5 T, 50 Hz and 2 T, 100 Hz operation points, respectively. As can be observed, for most of the cases the measured and computed maximum magnetic flux densities correspond very well. On the other hand, this implies that the FEM models have been correctly prepared, including the supply conditions. For the 2 T operation point, the laminated sample was measured for a slightly higher flux density, 2.16 T, which can be seen in Fig. 10. The additively manufactured samples were tested at 2 T.

For the grooved sample, the measured maximum magnetic flux densities were not reached in the simulations.

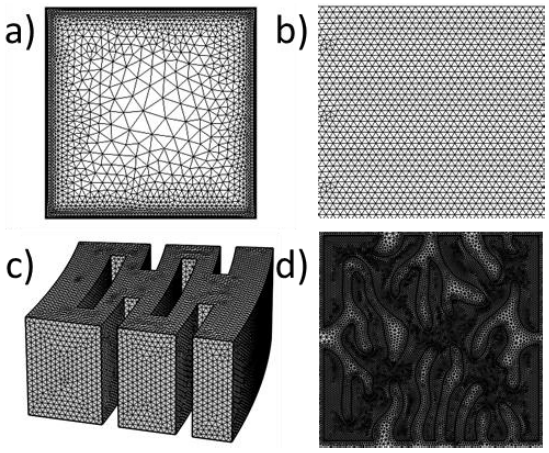

FIGURE 8. Finite element mesh used in a) the solid, b) the upper left corner of the laminated sample, c) the grooved sample case and d) for the TO DfAM sample for the operation point 2 T and 100 Hz.

This originates from the small geometrical discrepancies between the actual and modeled samples that are shown in Fig. 6 c and possibly from slight inhomogeneities caused by the 3D printing process. It is deduced that in combination, these effects are present in the simulations as different eddy-current behavior and AC magnetic characteristics, and consequently, lower magnetic flux densities at a given excitation.

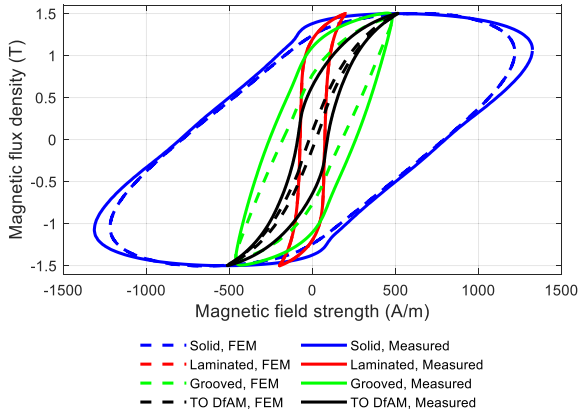

FIGURE 9. Measured and computed B-H curves at the 1.5 T, 50 Hz operation point.

The eddy current density in the four samples is shown in Fig. 11. In the solid core, the eddy currents form a large loop near the surface of the core. The laminated structure divides the large current loop into several small ones, which reduces the current density. The TO DfAM structure alters the path of the eddy current in such a way that the current density in the core is reduced, and therefore, the losses are mitigated.

Fig. 12 and Fig. 13 show computed eddy-current losses and measured total core losses in the solid sample and the laminated sample, respectively. For the solid core, the results are close to each other, and because the FEM model only takes into account the eddy-current losses, the results show

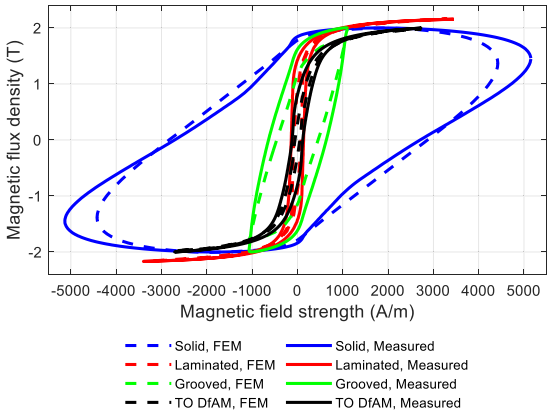

FIGURE 10. Measured and computed B-H curves at the 2 T, 100 Hz operation point.

that in solid cores, a major part of the losses is caused by the eddy currents. This result was expected, and it clarified that by mitigating the eddy currents in the core, the total core losses would also be significantly reduced. For the laminated core, the computed losses are less than half of its measured losses, which clearly shows the effects of laminations in eddy-current loss reduction. Compared with the solid sample, the losses are significantly smaller in the laminated sample, which underlines the need to develop a method to reduce the losses in the additively manufactured cores.

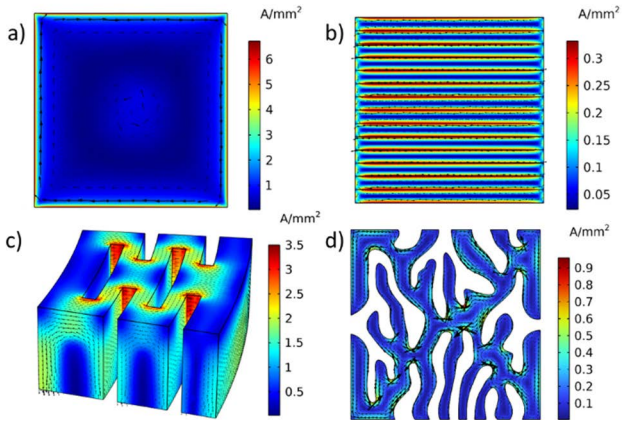

FIGURE 11. Eddy currents (at 2 T, 100 Hz) in (a) a solid sample, (b) a laminated sample, (c) a grooved sample, and (d) a TO DfAM sample.

Fig. 14 and Fig. 15 show the measured total core losses and the computed eddy-current losses for the grooved samples and the TO DfAM samples, respectively. Compared with the solid cores, the losses in the grooved cores are considerably smaller. For example, at 2 T, 100 Hz, the measured total core losses were reduced from 269 W/kg to 55 W/kg, which is an 80% reduction when compared with the solid core. However, when compared with the laminated sample, the losses are still not on the same level: the laminated sample losses are only 14 W/kg. Therefore, a better core design is needed.

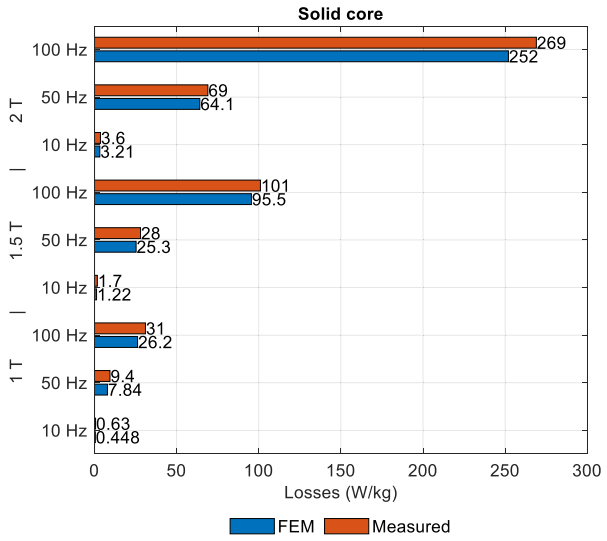

FIGURE 12. Measured total core losses and computed eddy-current losses in the solid core.

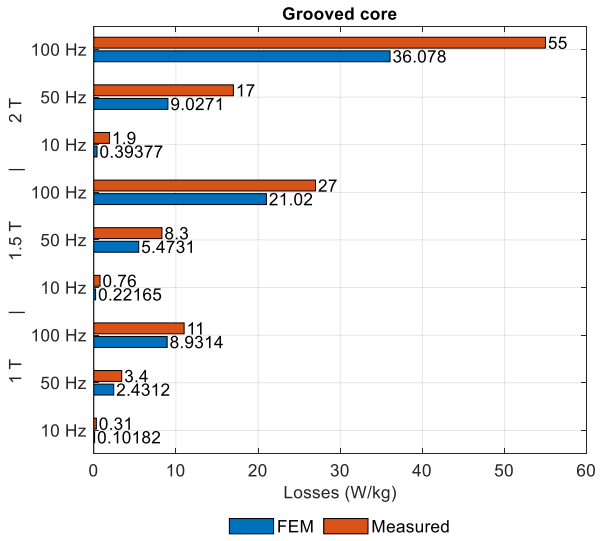

FIGURE 14. Measured total core losses and computed eddy-current losses in the grooved sample.

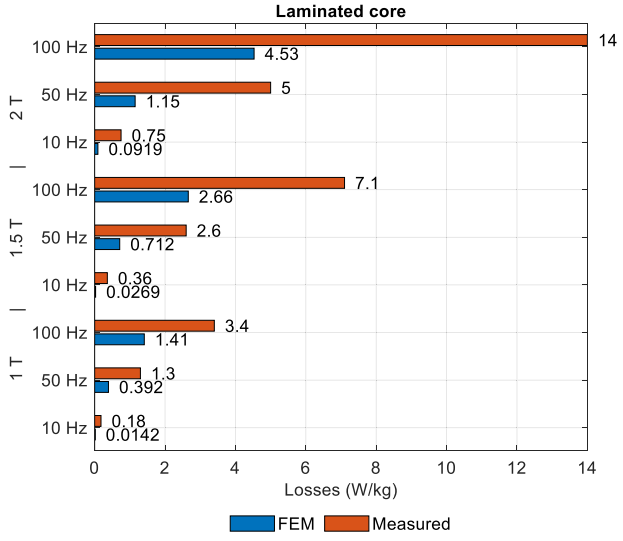

FIGURE 13. Measured total core losses and computed eddy-current losses in the laminated core.

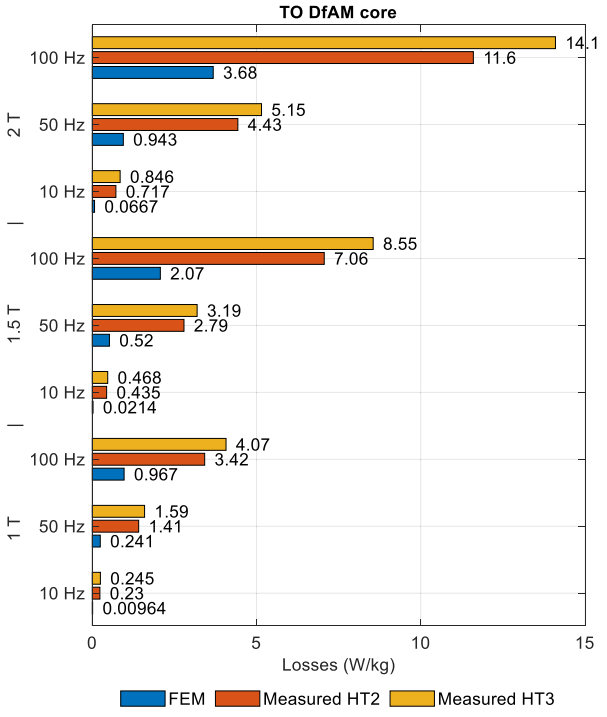

FIGURE 15. Measured total core losses and computed eddy-current losses in the TO DfAM cores.

For TO DfAM, two different measurement results are shown for two different heat treatments. The eddy-current losses are computed using the measured magnetic field values gained from the TO DfAM HT2 sample to obtain the primary current. When comparing the losses with those of the solid and laminated cores, it can be clearly seen that in the TO DfAM cores, the losses are on the same level as in the laminated cores. The laminated cores have measured losses of 14 W/kg, and the TO DfAM cores have losses of 11.6 W/kg for HT2 and 14.1 W/kg for HT3.

Fig. 16 shows the measured core losses as a percentage of the measured losses in the solid core. The higher the frequency is, the more loss reduction is obtained. This is reasonable because the eddy-current losses are more prominent at higher frequencies. The TO DfAM samples have similar capability for loss reduction to that of the laminated structure. There is only a clear difference in favor of the laminated sample for the smallest frequency, 10 Hz. The maximum reduction of losses was obtained at 2 T, 100 Hz, where losses were reduced to 4.3% of the losses in the solid core. The smallest reduction was 37% at 1 T, 10 Hz.

The computed secondary flux linkages for the operating points are shown in Fig. 17. It shows that the flux linkage of the grooved sample and of the TO DfAM sample is reduced

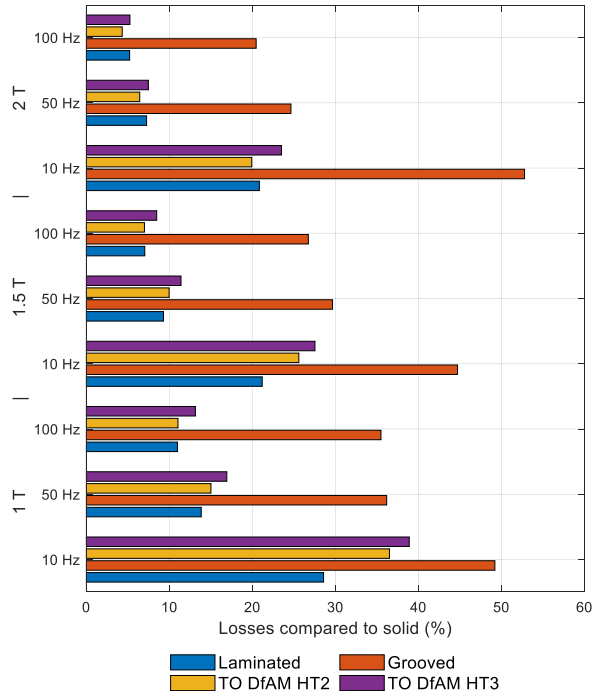

FIGURE 16. Measured losses (W/kg) relative to the solid sample.

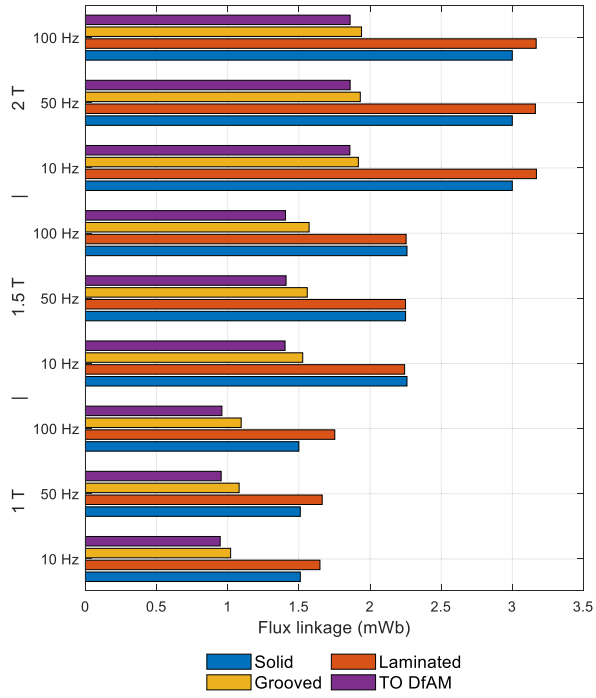

FIGURE 17. Flux linkage computed for the secondary winding of the different samples.

compared to the solid and the laminated sample due to the fact that introducing grooves or gaps to the structure reduces the cross-sectional area of the core. The solid core has slightly reduced flux linkage compared to the laminated one, because the eddy currents reduce the magnetic field in the solid core. The grooved core has slightly larger cross-sectional area which is why it has slightly larger flux linkage than the TO DfAM core. This difference in the flux linkage is significant and has to be taken into account when designing applications. What it could mean in practice is that if the application was built using the grooved or TO DfAM core type of structure, the outer dimensions should be made larger, to compensate the reduced cross-sectional area.

VI. CONCLUSION

We explore the design and preparation of functional additively manufactured ferromagnetic cores. The topic is important as it may enable the tailored, better performing electrical machines of the future and also streamlined processes with lower scrap. We studied if TO could be used to design loss-mitigating core structures for soft magnetic cores manufactured via PBF-LB. The TO was performed in 2D. The optimized cores were 3D printed, and the B-H characteristics and total core losses (W/kg) were measured. The eddy-current losses were solved with FEM. Both the measured total losses and the computed eddy-current losses were compared against the solid 3D-printed cores, the laminated cores, and the cores having 4 mm evenly placed grooves. The results show that the TO DfAM cores have losses that are comparable to those of the laminated cores, and significantly smaller losses when compared with the solid cores. When introducing gaps to the core, the core cross-sectional area is reduced, which has to be taken into account when designing cores for a real application such as an electrical motor. This can mean increased volume, but because the losses were evaluated as W/kg, the mass of the core should not increase.

Main challenge is that even though the TO produces a solution that effectively mitigates the eddy-current losses, the resulting core geometry can be difficult to manufacture by AM. This requires an additional design step that modifies the TO result for AM. However, this step was not too time consuming, and more importantly, it did not cause the design to lose its ability to mitigate the losses. To conclude, in this work, a new method for overcoming the challenge of the high eddy current losses in solid soft magnetic cores was implemented and proved to be efficient by both simulations and experiments. Further work is needed in order to take the manufacturability into account during the TO itself. In the future, we plan to test how applying this method in an actual application, such as an electrical motor, affects the performance of the application. By achieving high performance of the PBF-LB produced cores, the technology can in the future be competitive to laminated cores. This would provide a solution on how to manufacture soft magnetic cores especially for such applications that require 3D magnetic flux path, and therefore cannot be manufactured using laminated sheets.

REFERENCES

[1] J. Chen, D. Wang, S. Cheng, and J. Wang, "Influence of manufacture process on magnetic property of FeCoV alloy," in *Proc. 17th Int. Conf. Electr. Mach. Syst. (ICEMS)*, Oct. 2014, pp. 3054–3059.

[2] T. N. Lamichhane, L. Sethuraman, A. Dalagan, H. Wang, J. Keller, and M. P. Paranthaman, "Additive manufacturing of soft magnets for electrical machines—A review," *Mater. Today Phys.*, vol. 15, Dec. 2020, Art. no. 100255.

[3] V. Chaudhary, S. A. Mantri, R. V. Ramanujan, and R. Banerjee, "Additive manufacturing of magnetic materials," *Prog. Mater. Sci.*, vol. 114, May 2020, Art. no. 100688.

[4] T. I. El-Wardany, Y. She, V. N. Jagdale, J. K. Garofano, J. J. Liou, and W. R. Schmidt, "Challenges in three-dimensional printing of high-conductivity copper," *J. Electron. Packag.*, vol. 140, no. 2, pp. 1–12, Jun. 2018.

[5] F. Bittner, J. Thielsch, and W. G. Drossel, "Laser powder bed fusion of Nd–Fe–B permanent magnets," *Prog. Additive Manuf.*, vol. 5, no. 1, 2020, Art. no. 0123456789.

[6] H.-W. Jun, J.-W. Lee, G.-H. Yoon, and J. Lee, "Optimal design of the PMSM retaining plate with 3-D barrier structure and eddy-current loss-reduction effect," *IEEE Trans. Ind. Electron.*, vol. 65, no. 2, pp. 1808–1818, Feb. 2018.

[7] T. Riipinen, S. Metsä-Kortelainen, T. Lindroos, J. S. Keränen, A. Manninen, and J. Pippuri-Mäkeläinen, "Properties of soft magnetic Fe-Co-V alloy produced by laser powder bed fusion," *Rapid Prototyping J.*, vol. 25, no. 4, pp. 699–707, May 2019.

[8] D. Goll, J. Schurr, F. Trauter, J. Schanz, T. Bernthaler, H. Riegel, and G. Schneider, "Additive manufacturing of soft and hard magnetic materials," *Proc. CIRP*, vol. 94, pp. 248–253, Jan. 2020.

[9] J. Wang, X. Yuan, T. Riipinen, J. Pippuri-Makelainen, S. Metsa-Kortelainen, and T. Lindroos, "Evaluation of 3D printed cobalt iron cores for filter inductors," *IEEE Trans. Magn.*, vol. 56, no. 8, pp. 1–5, Aug. 2020.

[10] C. L. Cramer, P. Nandwana, J. Yan, S. F. Evans, A. M. Elliott, C. Chinnasamy, and M. P. Paranthaman, "Binder jet additive manufacturing method to fabricate near net shape crack-free highly dense Fe-6.5 wt.% Si soft magnets," *Heliyon*, vol. 5, no. 11, Nov. 2019, Art. no. e02804.

[11] E. Peng, X. Wei, T. S. Herng, U. Garbe, D. Yu, and J. Ding, "Ferrite-based soft and hard magnetic structures by extrusion free-forming," *RSC Adv.*, vol. 7, no. 43, pp. 27128–27138, 2017.

[12] F. Wu and A. M. El-Refaie, "Towards fully additively-manufactured permanent magnet synchronous machines: Opportunities and challenges," in *Proc. IEEE Int. Electr. Mach. Drives Conf. (IEMDC)*, May 2019, pp. 2225–2232.

[13] H. Tiismus, A. Kallaste, A. Belahcen, T. Vaimann, A. Rassõlkin, and D. Lukichev, "Hysteresis measurements and numerical losses segregation of additively manufactured silicon steel for 3D printing electrical machines," *Appl. Sci.*, vol. 10, no. 18, p. 6515, Sep. 2020.

[14] D. Goll, D. Schuller, G. Martinek, T. Kunert, J. Schurr, C. Sinz, T. Schubert, T. Bernthaler, H. Riegel, and G. Schneider, "Additive manufacturing of soft magnetic materials and components," *Additive Manuf.*, vol. 27, pp. 428–439, May 2019.

[15] S. Urbanek and B. Ponick, "Surface eddy current loss reduction in additively manufactured permanent magnet rotor active parts," in *Proc. 13th Int. Conf. Electr. Mach. (ICEM)*, Sep. 2018, pp. 1317–1322.

[16] H.-J. Pyo, J. W. Jeong, J. Yu, D.-W. Nam, S.-H. Yang, and W.-H. Kim, "Eddy current loss reduction in 3D-printed axial flux motor using 3D-printed SMC core," in *Proc. IEEE Energy Convers. Congr. Expo. (ECCE)*, Oct. 2020, pp. 1121–1125.

[17] M. P. Bendsøe, "Optimal shape design as a material distribution problem," *Struct. Optim.*, vol. 1, no. 4, pp. 193–202, 1989.

[18] D. N. Dyck and D. A. Lowther, "Automated design of magnetic devices by optimizing material distribution," *IEEE Trans. Magn.*, vol. 32, no. 3, pp. 1188–1192, May 1996.

[19] O. Sigmund and K. Maute, "Topology optimization approaches: A comparative review," *Struc. Multidiscipl. Optim.*, vol. 48, no. 6, pp. 1031–1055, Dec. 2013.

[20] M. P. Bendsøe and O. Sigmund, "Material interpolation schemes in topology optimization," *Arch. Appl. Mech.*, vol. 69, nos. 9–10, pp. 635–654, Nov. 1999.

[21] J. Lee, J. H. Seo, and N. Kikuchi, "Topology optimization of switched reluctance motors for the desired torque profile," *Struct. Multidisciplinary Optim.*, vol. 42, no. 5, pp. 783–796, 2010.

[22] F. Guo and I. P. Brown, "Multi-material magneto-structural topological optimization of wound field synchronous machines," in *Proc. IEEE Energy Convers. Congr. Expo. (ECCE)*, Sep. 2019, pp. 6516–6523.

[23] A. N. A. Hermann, N. Mijatovic, and M. L. Henriksen, "Topology optimisation of PMSM rotor for pump application," in *Proc. 22nd Int. Conf. Electr. Mach. (ICEM)*, Sep. 2016, pp. 2119–2125.

[24] S.-I. Park and S. Min, "Design of magnetic actuator with nonlinear ferromagnetic materials using level-set based topology optimization," *IEEE Trans. Magn.*, vol. 46, no. 2, pp. 618–621, Feb. 2010.

[25] Y. Okamoto, S. Wakao, and S. Sato, "Topology optimization based on regularized level-set function for solving 3-D nonlinear magnetic field system with spatial symmetric condition," *IEEE Trans. Magn.*, vol. 52, no. 3, pp. 1–4, Mar. 2016.

[26] P. Gangl, S. Amstutz, and U. Langer, "Topology optimization of electric motor using topological derivative for nonlinear magnetostatics," *IEEE Trans. Magn.*, vol. 52, no. 3, pp. 1–4, Mar. 2016.

[27] Y. Okamoto, R. Hoshino, S. Wakao, and T. Tsuburaya, "Improvement of torque characteristics for a synchronous reluctance motor using MMA-based topology optimization method," *IEEE Trans. Magn.*, vol. 54, no. 3, pp. 1–4, Mar. 2018.

[28] H. Masuda, Y. Okamoto, and S. Wakao, "Multistage topology optimization of induction heating apparatus in time domain electromagnetic field with magnetic nonlinearity," *COMPEL-Int. J. Comput. Math. Electr. Electron. Eng.*, vol. 38, no. 3, pp. 1009–1022, May 2019.

[29] *AMD2:2008 Amendment 2—Magnetic Materials—Part 4: Methods of Measurement of D.C. Magnetic Properties of Magnetically Soft Materials*, Standard IEC 60404-4:1995, 2008.

[30] K. Svanberg, "MMA and GCMMA—Two methods for nonlinear optimization," Optim. Syst. Theory, KTH, Stockholm, Sweden, 2007. [Online]. Available: https://people.kth.se/~krille/mmagcmma.pdf

[31] *COMSOL Multiphysics Web Page*. Accessed: Jul. 6, 2022. [Online]. Available: https://www.comsol.com/

[32] T. Riipinen, J. Pippuri-Mäkeläinen, T. Lindroos, S. Metsä-Kortelainen, J. S. Keränen, and A. Manninen, "Topology optimized soft magnetic cores by laser powder bed fusion," presented at the Euro PM Congr. Exhib., Maastricht, The Netherlands, 2019.

[33] VACUUMSCHMELZE. (2022). *Soft Magnetic Cobalt-Iron Alloys*. Accessed: Jan. 7, 2022. [Online]. Available: https://vacuumschmelze.com/03_Documents/Brochures/Cobalt-Iron_Alloys.pdf

[34] *AMD1:2021 Amendment 1—Magnetic Materials—Part 6: Methods of Measurement of the Magnetic Properties of Magnetically Soft Metallic and Powder Materials at Frequencies in the Range 20 Hz to 100 kHz by the Use of Ring Specimens*, Standard IEC 60404-6:2018, 2021.

AINO MANNINEN received the M.Sc. (Tech.) degree from Aalto University, Espoo, Finland, in 2012. She works as a Research Scientist at VTT Technical Research Centre of Finland Ltd., Espoo. Her research interests include the modeling of electrical machines and electrical powertrains, topology optimization, and the design of electrical machines for additive manufacturing.

JENNI PIPPURI-MÄKELÄINEN received the M.Sc. (Tech.) and D.Sc. (Tech.) degrees in electro mechanics, in 2003 and 2010, respectively. She works as a Principal Investigator and a Senior Scientist at VTT Technical Research Centre of Finland Ltd., Espoo, Finland. Prior to joining VTT, she was with Aalto University and ABB Corporate Research Center, Switzerland, as a Visiting Researcher. Her research interests include electrical machines, powertrains, and the design and optimization of electrical machinery for additive manufacturing.

TUOMAS RIIPINEN received the M.Sc. degree in materials science and engineering. He works as a Research Scientist at the Advanced Manufacturing Technologies Team, VTT Technical Research Centre of Finland Ltd. He has experience in material manufacturing and characterization methods. Since 2016, he has been working at VTT in the field of additive manufacturing (AM). He is currently focusing on laser powder bed fusion technology and metal materials. His research interests include AM includes material and process development and post-processing methods and additively manufactured magnetic materials for novel electrical machine designs.

TOMI LINDROOS received the M.Sc. (Tech.) degree in physical metallurgy and metal technology from the Tampere University of Technology, Tampere, Finland, in 2000. He works as a Research Team Leader at the Sustainable Materials Design Team, VTT Technical Research Centre of Finland Ltd., Tampere. He joined VTT in 1997, and after that, has worked in various roles in projects focused on materials and manufacturing. In 2007, he started as a Team Leader and, after that, has led different research groups consisting of researchers numbering from seven up to 33. Since 2003, he has been worked as a project manager and, later, also as a project coordinator and a project owner in multiple national and international research projects and working in projects directly funded by industry. He has been an IPMA C Certified Project Manager, since 2011. His research interests include powder-based material technologies and materials for additive manufacturing.

SINI METSÄ-KORTELAINEN received the D.Sc. (Tech.) degree from the School of Chemical Engineering, Aalto University. She works as a Research Team Leader and a Project Manager (IPMA C) at the Advanced Manufacturing Technologies Team, VTT Technical Research Centre of Finland Ltd., Espoo, Finland. She has 19 years of scientific experience. She has worked as a researcher and a manager in projects from the field of additive manufacturing (AM). She has experience of working with many kinds of AM materials, including metals, ceramics, and polymers—applied in a wide variety of applications ranging from the machine and processing industry to medical use.

ATTE ANTIKAINEN received the degree in materials science from the Tampere University of Technology, in 2017. He works as a Research Scientist at the Advanced Manufacturing Technologies Team, VTT Technical Research Centre of Finland Ltd. He joined VTT, in 2019. He has also worked with additive manufacturing while doing his master's thesis about heat treatments of DMLS titanium. His research interests include alloy development for different material groups such as tool steels and magnetic materials.